J. Plasma Physics (2006), *vol.* 72, *part* 3, *pp.* 359–382. © 2005 Cambridge University Press
doi:10.1017/S0022377805004149 First published online 7 December 2005 Printed in the United Kingdom

A three-dimensional analysis of the flow past an open terrestrial magnetopause

LARS G. WESTERBERG and HANS O. ÅKERSTEDT

Division of Fluid Mechanics, Luleå University of Technology, SE-971 87, Luleå, Sweden
(lgwe@itu.se)

(Received 1 July 2005 and accepted 1 August 2005)

Abstract. We present a three-dimensional analysis covering an investigation of the behavior of the magnetosheath plasma velocity and the magnetic field during the transfer from the magnetosheath to the magnetosphere. Magnetic reconnection is assumed to occur at an arbitrary line parallel to the y-axis, located in a region along the magnetopause stretching from the sub-solar point to the north. We do not focus on the process itself, but on its implications for the plasma flow and the magnetic field outside the diffusion region. Viscosity and resistivity are included in the magnetohydrodynamic equation of motion as non-ideal effects. The governing equations are solved approximately using the method of asymptotic expansions, with expansion in orders of large Reynolds and Lundquist numbers. We present two classes of solutions describing the properties north and south of the reconnection line, respectively. Results are presented for two locations of the reconnection line at distances of two and seven Earth radii from the sub-solar point correspondingly. It is shown that the velocity increases faster north of the reconnection line, and that the effect intensifies as the location of the reconnection line moves further away from the sub-solar point. It is also shown for this case, that there is less variation of the magnetic field and an increase in the field strength.

1. Introduction

At the beginning of the 1960s magnetic reconnection became a well-known concept in space physics. This was due to Dungey's (1961) pioneering work. However, the first contributions to this field was made by Ron Giovanelli around 1938 (Dungey 1995). The main ideas date from the work by Chapman and Ferraro (1931). Since then a tremendous amount of work has been carried out covering the spectra of magnetic reconnection. The first theoretical model treating slow reconnection was made by Sweet (1958) and Parker (1957). This model was then applied to solar flares. However, Parker found that the rate at which magnetic energy is transformed to kinetic energy is significantly too slow to be applicable to solar flares. A reconnection rate of about a factor of 100 was needed to explain the energy release. Petschek (1964) developed a model that could deal with higher reconnection rates, and therefore could be used in the application of solar flares. These contributors were followed by a couple of other significant scientists entering the stage of magnetic reconnection in the 1970s: Sonnerup (1970, 1979) and Yeh and Axford (1970). Their groundwork set the basis for subsequent work. During the last three decades there have been a huge number of contributors to this field of science (e.g. Vasyliunas

https://doi.org/10.1017/S0022377805004149 Published online by Cambridge University Press

1975; Cowley 1976, 1995; Heyn et al. 1983; Priest and Forbes 1986; Cowley and Owen 1989; Lee 1991).

A majority of the theoretical analysis work produced to the present day has concerned two dimensions. During the last two decades, as computational capacity has increased dramatically, most of the research treating the three-dimensional (3D) study of solar wind flow and magnetic reconnection, has focused on computer simulations and numerical analysis.

Lee (1991) gives a review of the different models proposed during the 45 year history of magnetic reconnection. Models of the diffusion region, inflow region and outflow region in two-dimensional (2D) steady-state reconnection, are reviewed. Some aspects of 3D reconnection are also covered, such as patchy reconnection and patchy multiple X-line reconnection. Recently, Ugai et al. (2004) considered a computer study of 3D fast reconnection, where they treated different resistivity parameter values. They showed that in the resulting 3D fast reconnection configuration, slow shocks stand and extend outwards in the finite extent. Ahead of the fast reconnection jet, a large-scale 3D plasmoid swells and propagates in the central current sheet, with the result that a vortex flow is formed near the plasmoid side boundary.

Wang et al. (2004) considered a 3D computational study of the plasma depletion layer formed at the sunward side of the magnetopause with lower plasma density and higher magnetic field compared to values further downstream along the magnetopause. They showed that a strong plasma pressure gradient force along the magnetic field at the bow shock and a pressure gradient force along the flux tube within the magnetosheath usually exist, pushing plasma away from the equatorial plane. (For other works see, for example, Ugai 1991; Büchner and Kuska 1997.)

Apart from its application to the terrestrial magnetopause, three-dimensional reconnection theory is also used in the analysis of the solar corona (see, for example, Priest 1997, 2003).

However, despite the fact that nowadays we are dealing with high-performance computing abilities, the need for theoretical models is still as important as ever. Partly because it creates a significant base for a wider understanding of the simulation results, but also because it is important for the development of new models.

The theoretical analysis of 3D reconnection had its beginnings at the end of the 1980s. The work of Hesse and Schindler (1988) together with Greene (1988) and Priest and Forbes (1989) represents a few of the earliest contributions. Also, the pioneering work by Dungey was influenced by his vision of a 3D magnetic and electric field (Dungey 1995). Cowley and Owen (1989) showed that reconnection is not limited to the vicinity of the sub-solar point. Furthermore, they showed that reconnection may occur for all relative directions of the magnetosheath magnetic field and magnetopause magnetic field, except when they are exactly parallel.

The present paper is a development of the work treating a 2D analysis of the solar wind flow past an open terrestrial magnetopause, done by Westerberg and Åkerstedt (2005), hereafter referred to as WÅ05. Which, in turn, was a development of the ideas presented by Cowley and Owen (1989). We consider reconnection to occur at an arbitrary line located at $z = z_0$. The onset of the reconnection process in the diffusion area is a highly interesting research topic, and is still under much discussion and debate among researchers. However, we do not focus on this issue. We assume that reconnection does occur, and follow the implications of this process outside the diffusion region.

https://doi.org/10.1017/S0022377805004149 Published online by Cambridge University Press

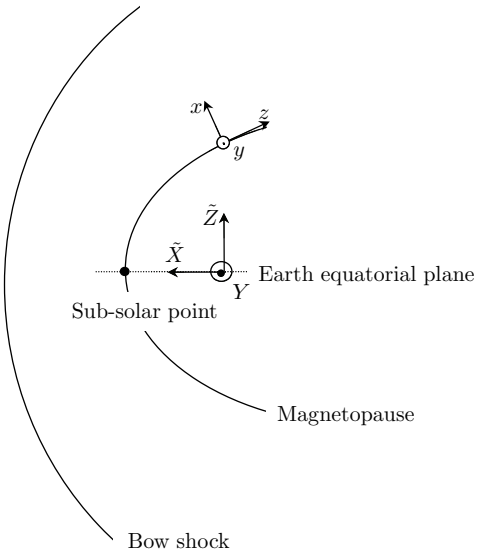


Figure 1. The curvilinear coordinate system, with the conventional label used in space physics for coordinate axis, i.e. at the sub-solar point; x pointing towards the Sun, z pointing from geographical south to north and y in a west to east direction. The reconnection line is located at $z = z_0$. The coordinate system with origin at the center of the Earth is used for the development of the parabolical unit vectors ($\hat{u}$, $\hat{v}$ and $\hat{\phi}$) in terms of the curvilinear coordinates x, y and z. See Sec. 3 for details.

The objective of this paper is to gain a description of the velocity and magnetic field in the magnetosheath region, and especially during the transition from the magnetosheath to the magnetopause.

The transition layer separating the magnetosheath plasma from the magnetosphere plasma is regarded to be very thin, implying that the magnetohydrodynamic (MHD) equations can be solved approximately using a perturbation expansion for large Reynolds (R) and Lundqvist (L_u) numbers. These are defined as

$$R = \frac{v_{\mathrm{A}} \cdot R_{\mathrm{E}}}{\nu} \tag{1.1}$$

and

$$L_u = \frac{v_{\mathrm{A}} \cdot R_{\mathrm{E}}}{\eta} \tag{1.2}$$

where ν is the kinematic viscosity of the magnetosheath plasma, η is the magnetic diffusivity and v_{A} is the Alfvén velocity at some reference point, which we have chosen to be located at one Earth radius from the sub-solar point. Viscosity and resistivity do not exist in the classical sense since the plasma is mainly collisionless, though we can treat them as anomalous transport coefficients. Axford (1964) estimated the kinematic viscosity to be $\nu = 10^{13}$ cm^2 s^{-1}. Haerendel et al. (1978) showed that the magnetic diffusivity is of the same order.

The conventional space physics coordinate system is used (see Fig. 1), where at the sub-solar point, x is pointing out of the paper, z is from geographical south to north and y in the west to east direction. Spreiter and Stahara (1980) showed that the magnetosheath velocity (at least locally) increases linearly away from the sub-solar

https://doi.org/10.1017/S0022377805004149 Published online by Cambridge University Press

point. However, their model does not include the effects of the magnetosheath magnetic field. The inclusion of a magnetic field causes a stagnation line, rather than a stagnation point, directed in coherence with the magnetic field (Farrugia et al. 1998). An exception is the case of aligned velocity and magnetic fields for which the flow is of stagnation point type.

The current paper is structured as follows. In Sec. 2 we define the dimensionless variables, state the governing equations and apply the perturbation expansion. This results in simplified equations describing the velocity and magnetic field in the transition layer near the reconnection line. In Sec. 3 the solutions to the equations are presented, while the results are presented in Sec. 4. We wrap it all up with the summary and conclusions in Sec. 5.

2. Transition layer analysis

2.1. The flow model and the thin-layer approximation

The magnetopause separating the magnetosheath plasma from the magnetosphere plasma is treated as a resolution of a rotational discontinuity for which the plasma motion can be considered incompressible. As in WÅ05 we only consider the current transition layer corresponding to the first large amplitude wave at the magnetopause boundary. Heyn et al. (1985) showed that the Alfvén wave is followed by a series of compressible waves in order to match the lower plasma density in the magnetosphere. In accordance with this, the plasma motion is considered to be governed by the incompressible MHD steady equation of motion,

$$\rho(\mathbf{u}\cdot\nabla)\mathbf{u} = \mu\nabla^2\mathbf{u} - \nabla P + \frac{1}{\mu_0}(\mathbf{B}\cdot\nabla)\mathbf{B} \tag{2.1}$$

where P is the total pressure

$$P = p + \frac{B^2}{2\mu_0}. \tag{2.2}$$

The magnetic field is described by the induction equation

$$\frac{\partial\mathbf{B}}{\partial t} = \nabla\times(\mathbf{u}\times\mathbf{B}) + \frac{1}{\mu_0\sigma}\nabla^2\mathbf{B}. \tag{2.3}$$

To complete the system we recall the property of incompressibility. This together with the solenoidal property of the magnetic field gives

$$\nabla\cdot\mathbf{u} = 0 \tag{2.4}$$

$$\nabla\cdot\mathbf{B} = 0. \tag{2.5}$$

Considering a three-dimensional flow we let

$$\mathbf{u} = u_x\hat{\mathbf{x}} + u_y\hat{\mathbf{y}} + u_z\hat{\mathbf{z}} \tag{2.6a}$$

$$\mathbf{B} = B_x\hat{\mathbf{x}} + B_y\hat{\mathbf{y}} + B_z\hat{\mathbf{z}}, \tag{2.6b}$$

where $\hat{\mathbf{x}},\hat{\mathbf{y}},\hat{\mathbf{z}}$ is a local plane coordinate system close to the reconnection line. The transition layer separating the magnetosheath plasma from the magnetosphere plasma is assumed to be thin, so δ^* is introduced as a characteristic thickness. The length scale in the main flow direction ($\hat{\mathbf{y}}$ and $\hat{\mathbf{z}}$) is taken as L. One choice of L being

https://doi.org/10.1017/S0022377805004149 Published online by Cambridge University Press

the Earth radius R_{E}. A small parameter δ

$$\delta = \frac{\delta^*}{R_{\mathrm{E}}} \ll 1 \tag{2.7}$$

is chosen.

An order of magnitude estimate shows that as in ordinary boundary layer theory the thickness scales as

$$\delta = O(R^{-1/2}). \tag{2.8}$$

The Lundquist number and the Reynolds number are from now on taken to be of the same order of magnitude. Dimensionless variables are introduced as follows:

$$\frac{u_x}{v_{\mathrm{A}}} \to u_x \tag{2.9a}$$

$$\frac{u_y}{v_{\mathrm{A}}} \to u_y \tag{2.9b}$$

$$\frac{u_z}{v_{\mathrm{A}}} \to u_z \tag{2.9c}$$

$$\frac{B_x}{B_0^*} \to B_x \tag{2.9d}$$

$$\frac{B_y}{B_0^*} \to B_y \tag{2.9e}$$

$$\frac{B_z}{B_0^*} \to B_z \tag{2.9f}$$

$$\frac{E_y}{v_{\mathrm{A}} \cdot B_0^*} \to E_y \tag{2.9g}$$

$$\frac{E_z}{v_{\mathrm{A}} \cdot B_0^*} \to E_z \tag{2.9h}$$

$$\frac{x}{R_{\mathrm{E}}} \to x \tag{2.9i}$$

$$\frac{y}{R_{\mathrm{E}}} \to y \tag{2.9j}$$

$$\frac{z}{R_{\mathrm{E}}} \to z. \tag{2.9k}$$

B_0^* is the z-component of the magnetic field along the magnetopause at one Earth radius from the sub-solar point. Recalling that

$$\frac{\partial}{\partial x} = O(R^{1/2}) \tag{2.10}$$

we introduce the new fast variable ξ,

$$\xi = R^{1/2} \cdot x \tag{2.11}$$

and

$$\frac{\partial}{\partial x} = R^{1/2} \frac{\partial}{\partial \xi}. \tag{2.12}$$

https://doi.org/10.1017/S0022377805004149 Published online by Cambridge University Press

2.1.1. Governing equations. Using the dimensionless variables and the fast variable ξ we obtain from the induction equation

$$\hat{\mathbf{y}} : R^{-1/2} \cdot \frac{\partial B_y}{\partial \xi} - u_\xi B_y + u_y B_\xi = E_z \tag{2.13a}$$

$$\hat{\mathbf{z}} : R^{-1/2} \cdot \frac{\partial B_z}{\partial \xi} - u_\xi B_z + u_z B_\xi = -E_y, \tag{2.13b}$$

where the Lundquist number is assumed to be of the same order as the Reynolds number. From the MHD equation of motion the corresponding equations are:

$$\begin{aligned}\hat{\xi} : \frac{\partial^2 u_\xi}{\partial \xi^2} + B_z \frac{\partial B_\xi}{\partial z} + B_y \frac{\partial B_\xi}{\partial y} + R^{-1/2} \cdot B_\xi \frac{\partial B_\xi}{\partial \xi} \\ = \frac{\partial P}{\partial \xi} + u_z \frac{\partial u_\xi}{\partial z} + u_y \frac{\partial u_\xi}{\partial y} + R^{-1/2} \cdot u_\xi \frac{\partial u_\xi}{\partial \xi}\end{aligned} \tag{2.14a}$$

$$\begin{aligned}\hat{\mathbf{y}} : \frac{\partial^2 u_y}{\partial \xi^2} + B_z \frac{\partial B_y}{\partial z} + B_y \frac{\partial B_y}{\partial y} + R^{-1/2} \cdot B_\xi \frac{\partial B_y}{\partial \xi} \\ = \frac{\partial P}{\partial y} + u_z \frac{\partial u_y}{\partial z} + u_y \frac{\partial u_y}{\partial y} + R^{-1/2} \cdot u_\xi \frac{\partial u_y}{\partial \xi}\end{aligned} \tag{2.14b}$$

$$\begin{aligned}\hat{\mathbf{z}} : \frac{\partial^2 u_z}{\partial \xi^2} + B_z \frac{\partial B_z}{\partial z} + B_y \frac{\partial B_z}{\partial y} + R^{-1/2} \cdot B_\xi \frac{\partial B_z}{\partial \xi} \\ = \frac{\partial P}{\partial z} + u_z \frac{\partial u_z}{\partial z} + u_y \frac{\partial u_z}{\partial y} + R^{-1/2} \cdot u_\xi \frac{\partial u_z}{\partial \xi}.\end{aligned} \tag{2.14c}$$

In the region outside the transition layer, corresponding to $R \to \infty$ and $L_u \to \infty$, we have for the induction equation

$$\hat{\mathbf{y}} : E_z + u_\xi B_y - u_y B_\xi = 0 \tag{2.15a}$$

$$\hat{\mathbf{z}} : E_y + u_z B_\xi - u_\xi B_z = 0 \tag{2.15b}$$

and correspondingly for the MHD equation of motion

$$\hat{\mathbf{y}} : \frac{\partial^2 u_y}{\partial \xi^2} + B_z \frac{\partial B_y}{\partial z} + B_y \frac{\partial B_y}{\partial y} = \frac{\partial P}{\partial y} + u_z \frac{\partial u_y}{\partial z} + u_y \frac{\partial u_y}{\partial y} \tag{2.16a}$$

$$\hat{\mathbf{z}} : \frac{\partial^2 u_z}{\partial \xi^2} + B_z \frac{\partial B_z}{\partial z} + B_y \frac{\partial B_z}{\partial y} = \frac{\partial P}{\partial z} + u_z \frac{\partial u_z}{\partial z} + u_y \frac{\partial u_z}{\partial y}. \tag{2.16b}$$

Equations (2.4) and (2.5) complete the system,

$$R^{1/2} \cdot \frac{\partial u_\xi}{\partial \xi} + \frac{\partial u_y}{\partial y} + \frac{\partial u_z}{\partial z} = 0 \tag{2.17a}$$

$$R^{1/2} \cdot \frac{\partial B_\xi}{\partial \xi} + \frac{\partial B_y}{\partial y} + \frac{\partial B_z}{\partial z} = 0. \tag{2.17b}$$

2.2. The perturbation expansion and the DeHoffmann–Teller frame of reference

The absolute velocities in the main flow directions are divided into a DeHoffmann–Teller velocity, and the velocity with respect to the DeHoffmann–Teller frame of reference (DeHoffmann and Teller 1950), such that

$$u_y^* = u_y + U_{y\,\mathrm{HT}} \tag{2.18a}$$

$$u_z^* = u_z + U_{z\,\mathrm{HT}}. \tag{2.18b}$$

https://doi.org/10.1017/S0022377805004149 Published online by Cambridge University Press

U_{yHT} and U_{zHT} are hereafter referred to as U_y and U_z, respectively. They are chosen such that

$$E_y + B_x^{(0)} U_z = 0 \tag{2.19a}$$

$$E_z - B_x^{(0)} U_y = 0. \tag{2.19b}$$

In the DeHoffmann–Teller frame the plasma properties – except for the magnetic field and the direction of the plasma flow – are the same on both sides of the magnetopause, i.e. in the magnetosheath and the boundary layer. Furthermore, the electric field is zero in both the y and z directions, implying that the particles do not change their kinetic energy when passing through the current sheath from one side to another.

For the solution we apply the following perturbation expansion:

$$u_\xi = R^{-1/4} \cdot u_\xi^{(0)} + R^{-1/2} \cdot u_\xi^{(1)} + \cdots \tag{2.20a}$$

$$u_y = u_y^{(0)} + R^{-1/4} \cdot u_y^{(1)} + U_y + \cdots \tag{2.20b}$$

$$u_z = u_z^{(0)} + R^{-1/4} \cdot u_z^{(1)} + U_z + \cdots \tag{2.20c}$$

$$B_\xi = R^{-1/4} \cdot B_\xi^{(0)} + R^{-1/2} \cdot B_\xi^{(1)} + \cdots \tag{2.20d}$$

$$B_y = B_y^{(0)} + R^{-1/4} \cdot B_y^{(1)} + \cdots \tag{2.20e}$$

$$B_z = B_z^{(0)} + R^{-1/4} \cdot B_z^{(1)} + \cdots . \tag{2.20f}$$

The electric field and therefore the reconnection rate, are considered to be of order $O(R^{-1/4})$. However, it can be shown that any other ordering which goes to zero slower than $O(R^{-1/2})$ leads to the same set of equations. For instance, the reconnection rate by Petschek of order $O((\log R)^{-1})$ and the reconnection rate by Sonnerup of order $O(1)$ fulfill the requirement. Since the reconnection rate for the present application at the dayside magnetopause with asymmetric plasma densities in the magnetosheath and the magnetopause is not known to the authors, we will consider the ordering $O(R^{-1/4})$.

2.3. Properties north and south of the reconnection line

The MHD equation of motion (2.14) gives to order $O(R^{1/4})$

$$u_\xi^{(0)} \frac{\partial u_y^{(0)}}{\partial \xi} = B_\xi^{(0)} \frac{\partial B_y^{(0)}}{\partial \xi}. \tag{2.21}$$

To order $O(R^{1/4})$ (2.17) gives

$$u_\xi^{(0)} = u_\xi^{(0)}(y, z) \tag{2.22a}$$

$$B_\xi^{(0)} = B_\xi^{(0)}(y, z) \tag{2.22b}$$

that is, the lowest order of the tangential component of the velocity and the magnetic field, is independent of ξ. To lowest order of (2.13a) we obtain

$$u_y^{(0)} = \frac{B_y^{(0)} \cdot u_\xi^{(0)}}{B_\xi^{(0)}} \tag{2.23a}$$

$$u_z^{(0)} = \frac{B_z^{(0)} \cdot u_\xi^{(0)}}{B_\xi^{(0)}}, \tag{2.23b}$$

https://doi.org/10.1017/S0022377805004149 Published online by Cambridge University Press

which together with (2.22) and (2.21) gives two cases which we refer to conditions north and south of the reconnection line, respectively.

Northern reconnection

$$\begin{aligned} u_\xi^{(0)} &= B_\xi^{(0)} \\ u_y^{(0)} &= B_y^{(0)} \\ u_z^{(0)} &= B_z^{(0)}. \end{aligned} \tag{2.24}$$

Southern reconnection

$$\begin{aligned} u_\xi^{(0)} &= -B_\xi^{(0)} \\ u_y^{(0)} &= -B_y^{(0)} \\ u_z^{(0)} &= -B_z^{(0)}. \end{aligned} \tag{2.25}$$

In the further analysis these conditions are used to derive equations describing properties north and south of the reconnection line. From $O(R^0)$ of (2.14) together with (2.22) we can verify one fundamental property of the transition layer

$$\frac{\partial P}{\partial \xi} = 0, \tag{2.26}$$

i.e. the total pressure is constant through the transition layer. In order to obtain the equations of the velocity distribution for the northern and southern reconnection case we use (2.5) and (2.4) to $O(R^0)$, giving

$$\frac{\partial B_\xi^{(1)}}{\partial \xi} + \frac{\partial B_y^{(0)}}{\partial y} + \frac{\partial B_z^{(0)}}{\partial z} = 0 \tag{2.27a}$$

$$\frac{\partial u_\xi^{(1)}}{\partial \xi} + \frac{\partial u_y^{(0)}}{\partial y} + \frac{\partial U_y}{\partial y} + \frac{\partial u_z^{(0)}}{\partial z} + \frac{\partial U_z}{\partial z} = 0. \tag{2.27b}$$

2.3.1. Conditions north of the reconnection line. By subtracting (2.27b) from (2.27a), using the properties for the northern reconnection case (2.24) this results in the relation

$$u_\xi^{(1)} - B_\xi^{(1)} = -\left(\frac{\partial U_y}{\partial y} + \frac{\partial U_z}{\partial z}\right) \cdot \xi + f(y,z) \tag{2.28}$$

where the function f can be chosen as zero. Differentiating the y-component of $O(R^{-1/2})$ of the induction equation with respect to ξ, subtracting the result from $O(R^0)$ of the y-component of the MHD equation of motion using (2.24) and (2.28), results in the equation describing properties north of a reconnection line in the y-direction,

$$\begin{aligned} \hat{\mathbf{y}} : 2\frac{\partial^2 u_y^{(0)}}{\partial \xi^2} + 2\xi\left(\frac{\partial U_y}{\partial y} + \frac{\partial U_z}{\partial z}\right)\frac{\partial u_y^{(0)}}{\partial \xi} + u_y^{(0)}\frac{\partial U_z}{\partial z} - 2U_y\frac{\partial u_y^{(0)}}{\partial y} \\ - U_y\frac{\partial u_z^{(0)}}{\partial z} - U_y\frac{\partial U_y}{\partial y} - u_z^{(0)}\frac{\partial U_y}{\partial z} - U_z\left(\frac{\partial u_y^{(0)}}{\partial z} + \frac{\partial U_y}{\partial z}\right) - \frac{\partial P}{\partial y} = 0. \end{aligned} \tag{2.29}$$

The corresponding z-component is obtained through the same procedure as above, using the same order as in the previous case of the z-component of the induction

https://doi.org/10.1017/S0022377805004149 Published online by Cambridge University Press

equation and the MHD equation of motion, together with (2.24) and (2.28). This results in

$$\hat{\mathbf{z}}: 2\frac{\partial^2 u_z^{(0)}}{\partial \xi^2} + 2\xi\left(\frac{\partial U_y}{\partial y} + \frac{\partial U_z}{\partial z}\right)\frac{\partial u_z^{(0)}}{\partial \xi} + u_z^{(0)}\frac{\partial U_y}{\partial y} - 2U_z\frac{\partial u_z^{(0)}}{\partial z} - U_z\frac{\partial u_y^{(0)}}{\partial y} - U_y\left(\frac{\partial u_z^{(0)}}{\partial y} + \frac{\partial U_z}{\partial y}\right) - U_z\frac{\partial U_z}{\partial z} - u_y^{(0)}\frac{\partial U_z}{\partial y} - \frac{\partial P}{\partial z} = 0. \quad (2.30)$$

Equations (2.29) and (2.30) can also be derived using a solvability condition as in WÅ05. We note that (2.29) and (2.30) are linear, in comparison to the nonlinear equation (2.1).

2.3.2. Conditions south of the reconnection line. By adding (2.27a) and (2.27b), using the relation for the condition south of a reconnection line (2.24), we obtain the corresponding relation to the northern case

$$u_\xi^{(1)} + B_\xi^{(1)} = -\left(\frac{\partial U_y}{\partial y} + \frac{\partial U_z}{\partial z}\right)\cdot \xi + g(y,z) \quad (2.31)$$

where the function g can be chosen as zero. Following the same procedure as for the derivation of (2.29) and (2.30) we obtain the equations describing the properties south of a reconnection line. However, these are identical to the equations treating the northern case. Although the equations are the same for both cases, the DeHoffmann–Teller velocities are different depending on which case is taken into consideration, resulting in different governing equations for the northern and southern cases.

3. Solutions

3.1. Velocity and magnetic field along the magnetopause

As in WÅ05 we wish to match asymptotically the solutions of the equations describing the transition with solutions describing the magnetosheath plasma.

In WÅ05 we derived 3D irrotational solutions describing the magnetosheath velocity and magnetic fields with given paraboloidal shape of the bow shock and the magnetopause. To ensure that these solutions satisfy Ohm's law the electric field must vanish and the velocity and the magnetic field must be aligned. The solutions are therefore approximations in the limit of weak reconnection. These solutions are given in parabolical coordinates as:

$$\mathbf{U}^* = M_\mathrm{A} R_\mathrm{mp}\sqrt{\frac{u}{u+1}}\hat{\mathbf{u}} \quad (3.1a)$$

$$\mathbf{B}^* = -R_\mathrm{mp}\sqrt{\frac{u}{u+1}}\hat{\mathbf{u}} \quad (3.1b)$$

where

$$\hat{\mathbf{u}} = \sqrt{\frac{v}{u+v}}\cdot\cos\phi\hat{\mathbf{Y}} + \sqrt{\frac{v}{u+v}}\cdot\sin\phi\hat{\tilde{Z}} - \hat{\mathbf{X}} \quad (3.2a)$$

$$\hat{\mathbf{v}} = \sqrt{\frac{u}{u+v}}\cdot\cos\phi\hat{\mathbf{Y}} + \sqrt{\frac{u}{u+v}}\cdot\sin\phi\hat{\tilde{Z}} + \hat{\mathbf{X}} \quad (3.2b)$$

$$\hat{\phi} = -\sin\phi\hat{\mathbf{Y}} + \cos\phi\hat{\tilde{\mathbf{Z}}} \quad (3.2c)$$

https://doi.org/10.1017/S0022377805004149 Published online by Cambridge University Press

u, v and ϕ are the parabolical coordinates with the metric defined in WÅ05. X, Y and $\tilde{Z}$ (not to be confused with the new z variable Z, introduced in the next section) are the coordinates in the fixed system, while x, y and z are the curvilinear coordinates (see Fig. 1). Introducing a local coordinate system at the location of the reconnection line ($u = u_0$, $v = 1$, $\phi = \pi/2$) gives

$$\hat{\mathbf{u}}(u_0, v = 1, \phi = \pi/2) = \sqrt{\frac{1}{u_0 + 1}}\hat{\tilde{\mathbf{Z}}} - \hat{\mathbf{X}} = \hat{\mathbf{z}} \tag{3.3a}$$

$$\hat{\mathbf{v}}(u_0, v = 1, \phi = \pi/2) = \sqrt{\frac{u_0}{u_0 + 1}}\hat{\tilde{\mathbf{Z}}} + \hat{\mathbf{X}} = \hat{\mathbf{x}} \tag{3.3b}$$

$$\hat{\phi}(u_0, v = 1, \phi = \pi/2) = -\hat{\mathbf{Y}} = -\hat{\mathbf{y}}. \tag{3.3c}$$

By expanding for small ϕ we obtain

$$\hat{\mathbf{u}} = \hat{\mathbf{z}} + \frac{y}{R_{\mathrm{mp}}\sqrt{u \cdot (u + 1)}}\hat{\mathbf{y}} \tag{3.4a}$$

$$\hat{\phi} = -\hat{\mathbf{Y}} = -\hat{\mathbf{y}} \tag{3.4b}$$

$$\Delta\phi = \frac{y}{R_{\mathrm{mp}}\sqrt{u}}. \tag{3.4c}$$

This results in

$$B_y^* = -\frac{1}{u + 1} \cdot y \tag{3.5a}$$

$$B_z^* = -R_{\mathrm{mp}}\sqrt{\frac{u}{u + 1}} \tag{3.5b}$$

$$U_y^* = \frac{M_{\mathrm{A}}}{u + 1} \cdot y \tag{3.5c}$$

$$U_z^* = M_{\mathrm{A}} R_{\mathrm{mp}}\sqrt{\frac{u}{u + 1}}. \tag{3.5d}$$

Expansion for small u near the location of the reconnection line u_0, together with the relation between u and Z gives

$$dZ = h_u\, du = \frac{R_{\mathrm{mp}}}{2}\sqrt{\frac{u_0 + 1}{u_0}}(u - u_0), \tag{3.6}$$

where $Z = (z - z_0)$ and h_u is the scale-factor between Z and u. Equation (3.5) then becomes

$$B_y^* = -\frac{1}{u_0 + 1} \cdot y \tag{3.7a}$$

$$B_z^* = -R_{\mathrm{mp}}\sqrt{\frac{u_0}{u_0 + 1}} - \frac{1}{(u_0 + 1)^2} \cdot Z \tag{3.7b}$$

$$U_y^* = \frac{M_{\mathrm{A}}}{u_0 + 1} \cdot y \tag{3.7c}$$

$$U_z^* = R_{\mathrm{mp}} M_{\mathrm{A}}\sqrt{\frac{u_0}{u_0 + 1}} + \frac{M_{\mathrm{A}}}{(u_0 + 1)^2} \cdot Z. \tag{3.7d}$$

https://doi.org/10.1017/S0022377805004149 Published online by Cambridge University Press

3.2. The self-similar solution and expansion of the DeHoffmann–Teller velocity

We proceed to find solutions of (2.29) and (2.30). The DeHoffmann–Teller velocities are expanded such that

$$U_y = Q_y \cdot y \tag{3.8a}$$

$$U_z = U_z^0 + Q_z \cdot (z - z_0), \tag{3.8b}$$

where U_z^0 is the DeHoffmann–Teller velocity at the reconnection line ($z = z_0$) and $Q_{y,z}$ is the DeHoffmann–Teller velocity gradient in the respective direction. $u_y^{(0)}$ is developed such that $u_y^{(0)} = y\bar{u}_y^{(0)}$, where $\bar{u}_y^{(0)}$ is of order $O(1)$. We note that (2.29) and (2.30) are of parabolic type, so we seek to find a self-similar solution where

$$\eta = \xi \cdot g(z) \tag{3.9a}$$

$$Z = z - z_0. \tag{3.9b}$$

The function g is the inverse of the transition layer thickness (δ). This gives the partial derivatives

$$\frac{\partial}{\partial z} = \frac{\partial}{\partial Z}\frac{\partial Z}{\partial z} + \frac{\partial}{\partial \eta}\frac{\partial \eta}{\partial z} = \frac{\partial}{\partial Z} + \frac{\partial}{\partial \eta}\frac{\eta}{g}\cdot g'(z) \tag{3.10a}$$

$$\frac{\partial}{\partial \xi} = \frac{\partial}{\partial \eta}\frac{\partial \eta}{\partial \xi} = g(z)\frac{\partial}{\partial \eta} \tag{3.10b}$$

$$\frac{\partial^2}{\partial \xi^2} = g^2\frac{\partial^2}{\partial \eta^2} \tag{3.10c}$$

resulting in the new set of equations

$$\begin{aligned}\hat{\mathbf{z}} : {} & 2g^2\frac{\partial^2 u_z^{(0)}}{\partial \eta^2} + 2\eta\cdot(Q_y + Q_z)\frac{\partial u_z^{(0)}}{\partial \eta} + Q_y u_z^{(0)} \\ & - 2(U_z^0 + Q_z\cdot Z)\cdot\left(\frac{\partial u_z^{(0)}}{\partial Z} + \frac{\eta g'}{g}\frac{\partial u_z^{(0)}}{\partial \eta}\right) - (U_z^0 + Q_z\cdot Z)\cdot\bar{u}_y^{(0)} \\ & - Q_y y\cdot\frac{\partial u_z^{(0)}}{\partial y} - Q_z(U_z^0 + Q\cdot Z) - \frac{\partial P}{\partial Z} = 0\end{aligned} \tag{3.11a}$$

$$\begin{aligned}\hat{\mathbf{y}} : {} & 2g^2\frac{\partial^2 (y u_y^{(0)})}{\partial \eta^2} + 2\eta\cdot(Q_y + Q_z)\frac{\partial (y u_y^{(0)})}{\partial \eta} \\ & + Q_z y\cdot\bar{u}_y^{(0)} - Q_y y\cdot\left(\frac{\partial u_z^{(0)}}{\partial Z} + \frac{\eta g'}{g}\frac{\partial u_z^{(0)}}{\partial \eta}\right) - 2Q_y y\cdot\bar{u}_y^{(0)} - Q_y^2 y \\ & - (U_z^0 + Q_z\cdot Z)\cdot\left[\frac{\partial (y\bar{u}_y^{(0)})}{\partial Z} + \frac{\eta g'}{g}\frac{\partial (y\bar{u}_y^{(0)})}{\partial \eta}\right] - \frac{\partial P}{\partial y} = 0.\end{aligned} \tag{3.11b}$$

We obtain the pressure by considering the inviscid MHD equation of motion, i.e. the equation valid in the magnetosheath region

$$u_y\frac{\partial u_z}{\partial y} + u_z\frac{\partial u_z}{\partial Z} = -\frac{\partial P}{\partial Z} + B_y\frac{\partial B_z}{\partial y} + B_z\frac{\partial B_z}{\partial Z} \tag{3.12a}$$

$$u_y\frac{\partial u_y}{\partial y} + u_z\frac{\partial u_y}{\partial Z} = -\frac{\partial P}{\partial y} + B_y\frac{\partial B_y}{\partial y} + B_z\frac{\partial B_y}{\partial Z}. \tag{3.12b}$$

https://doi.org/10.1017/S0022377805004149 Published online by Cambridge University Press

3.3. Velocity gradients and the DeHoffmann–Teller velocity

The velocity and magnetic field in the magnetosheath are given by (3.7), where

$$U_y^* = U_y + \lim_{\eta\to\infty} u_y^{(0)} \tag{3.13a}$$

$$U_z^* = U_z + \lim_{\eta\to\infty} u_z^{(0)}. \tag{3.13b}$$

North and south of the reconnection line we therefore have

$$U_y^* = U_y^{\mathrm{N}} + \lim_{\eta\to\infty} B_y^{(0)} \tag{3.14a}$$

$$U_z^* = U_z^{\mathrm{N}} + \lim_{\eta\to\infty} B_z^{(0)} \tag{3.14b}$$

$$U_y^* = U_y^{\mathrm{S}} - \lim_{\eta\to\infty} B_y^{(0)} \tag{3.14c}$$

$$U_z^* = U_z^{\mathrm{S}} - \lim_{\eta\to\infty} B_z^{(0)} \tag{3.14d}$$

i.e.

$$\mathbf{U}^* = \mathbf{U}^{\mathrm{N}} + \mathbf{B}^* \tag{3.15a}$$

$$\mathbf{U}^* = \mathbf{U}^{\mathrm{S}} - \mathbf{B}^* \tag{3.15b}$$

where N and S correspond to north and south of the reconnection line, respectively. Equation (3.7) together with (3.14) gives

$$U_y^{\mathrm{N}} = (M_{\mathrm{A}} + 1) \cdot \frac{y}{u_0 + 1} \tag{3.16a}$$

$$U_z^{\mathrm{N}} = (M_{\mathrm{A}} + 1) \cdot \left[R_{\mathrm{mp}} \sqrt{\frac{u_0}{u_0 + 1}} + \frac{Z}{(u_0 + 1)^2} \right] \tag{3.16b}$$

$$U_y^{\mathrm{S}} = (M_{\mathrm{A}} - 1) \cdot \frac{y}{u_0 + 1} \tag{3.16c}$$

$$U_z^{\mathrm{S}} = (M_{\mathrm{A}} - 1) \cdot \left[R_{\mathrm{mp}} \sqrt{\frac{u_0}{u_0 + 1}} - \frac{Z}{(u_0 + 1)^2} \right]. \tag{3.16d}$$

This results for the velocity gradients in:

North of the reconnection line

$$\hat{\mathbf{y}}: \quad Q^* = \frac{M_{\mathrm{A}}}{u_0 + 1} \tag{3.17a}$$

$$Q_B = -\frac{1}{u_0 + 1} \tag{3.17b}$$

$$Q = \frac{M_{\mathrm{A}} + 1}{u_0 + 1} \tag{3.17c}$$

$$\hat{\mathbf{z}}: \quad Q^* = \frac{M_{\mathrm{A}}}{u_0 + 1} \tag{3.17d}$$

$$Q_B = -\frac{1}{(u_0 + 1)^2} \tag{3.17e}$$

$$Q = \frac{M_{\mathrm{A}} + 1}{(u_0 + 1)^2} \tag{3.17f}$$

https://doi.org/10.1017/S0022377805004149 Published online by Cambridge University Press

South of the reconnection line

$$\hat{\mathbf{y}}: \quad Q^* = \frac{M_\mathrm{A}}{u_0+1} \tag{3.18a}$$

$$Q_B = -\frac{1}{u_0+1} \tag{3.18b}$$

$$Q = \frac{M_\mathrm{A}-1}{u_0+1} \tag{3.18c}$$

$$\hat{\mathbf{z}}: \quad Q^* = \frac{M_\mathrm{A}}{u_0+1} \tag{3.18d}$$

$$Q_B = -\frac{1}{(u_0+1)^2} \tag{3.18e}$$

$$Q = \frac{1-M_\mathrm{A}}{(u_0+1)^2}. \tag{3.18f}$$

3.4. The perturbation expansion

For the solutions to (3.11) we expand the velocities and the function g such that

$$u_z^{(0)} = f_0(\eta) + Z \cdot f_1(\eta) + \cdots \tag{3.19a}$$

$$\bar{u}_y^{(0)} = g_0(\eta) + \cdots \tag{3.19b}$$

$$2g^2 = \frac{k_1}{Z} + \cdots \tag{3.19c}$$

$$\frac{g'}{g} = \frac{\frac{d}{dz}(g^2)}{2g^2} = -\frac{1}{2Z} + \cdots \tag{3.19d}$$

where k_1 is an arbitrary constant. Applying (3.19) in (3.11) results in the following orders:

$$O(Z^{-1}): k_1 \frac{\partial^2 f_0}{\partial \eta^2} + U_z^0 \eta \frac{\partial f_0}{\partial \eta} = 0 \tag{3.20a}$$

$$k_1 \frac{\partial^2 g_0}{\partial \eta^2} + \frac{U_z^0}{2} \eta \frac{\partial g_0}{\partial \eta} = \frac{Q_y}{2} \eta \frac{\partial f_0}{\partial \eta} \tag{3.20b}$$

$$O(Z^0): k_1 \frac{\partial^2 f_1}{\partial \eta^2} + U_z^0 \eta \frac{\partial f_1}{\partial \eta} - 2U_z^0 f_1 = -k_2 \frac{\partial^2 f_0}{\partial \eta^2} - (3Q_y - 4k_2)\eta \frac{\partial f_0}{\partial \eta} - Q_y f_0 + U_z^0 (g_0 + Q_z). \tag{3.20c}$$

Choosing $k_1 = U_z^0/4$ results in the solutions for f_0 and g_0,

$$f_0(\eta) = C_1 + C_2 \cdot \mathrm{erf}(\sqrt{2}\eta) \tag{3.21a}$$

$$g_0(\eta) = C_4 - \frac{Q_y C_2}{U_z^0} \cdot \mathrm{erf}(\sqrt{2}\eta) + \frac{\sqrt{\pi} C_3}{2} \cdot \mathrm{erf}(\eta). \tag{3.21b}$$

3.5. Asymptotic matching

Having obtained the lowest-order solutions, we want to match these at the location of the reconnection site (i.e. $Z = 0$) with the outer ($\eta \to \infty$) and inner ($\eta \to -\infty$) properties of the components of the velocity and the magnetic field, in order to obtain the complete solution, including the expressions for C_1 to C_4. Two characteristic solutions valid north and south of the reconnection line respectively, occur.

https://doi.org/10.1017/S0022377805004149 Published online by Cambridge University Press

3.5.1. North of the reconnection line. In order to match the solutions, we consider the boundary conditions for each parameter listed below. The value of the magnetic field immediately inside the magnetopause is set to 70 nT (Merrill et al. 1996). This is a good approximation in order to estimate the ratio between the outer and inner magnetic field strength at different locations of the reconnection site. In order to obtain the dimensionless quantity, the magnetic field strength is scaled using the factor

$$B_x^{\mathrm{imf}} \cdot \frac{\nu_{\mathrm{bs}}}{\nu_{\mathrm{bs}} - 1} \tag{3.22}$$

where $\nu_{\mathrm{bs}} = 1.25 R_{\mathrm{mp}}$ is the distance to the bow shock (WÅ05). The outer magnetic field is zero at the sub-solar point, while it increases linearly with the distance away from the sub-solar point.

In this analysis we consider two locations of the reconnection line; 2 and $7R_{\mathrm{E}}$ from the sub-solar point, respectively. This results in a ratio of $B_z^{\mathrm{outer}}/B_z^{\mathrm{inner}} = 1$ and $B_z^{\mathrm{outer}}/B_z^{\mathrm{inner}} = 2$ for the respective cases. The following boundary conditions at the respective reconnection sites are therefore considered.

Reconnection line at two Earth radii from the sub-solar point:

$$\eta \to -\infty: \quad B_z^{(0)} = R_{\mathrm{mp}} \sqrt{\frac{u_0}{u_0 + 1}} \tag{3.23a}$$

$$B_y^{(0)} = 0 \tag{3.23b}$$

$$\eta \to +\infty: \quad B_z^{(0)} = -R_{\mathrm{mp}} \sqrt{\frac{u_0}{u_0 + 1}} \tag{3.23c}$$

$$B_y^{(0)} = u_y^{(0)} = U_y^* - U_y^{\mathrm{N}} = -\frac{1}{(u_0 + 1)} \cdot y. \tag{3.23d}$$

Reconnection line at seven Earth radii from the sub-solar point:

$$\eta \to -\infty: \quad B_z^{(0)} = \frac{1}{2} \cdot R_{\mathrm{mp}} \sqrt{\frac{u_0}{u_0 + 1}} \tag{3.24a}$$

$$B_y^{(0)} = 0 \tag{3.24b}$$

$$\eta \to +\infty: \quad B_z^{(0)} = -R_{\mathrm{mp}} \sqrt{\frac{u_0}{u_0 + 1}} \tag{3.24c}$$

$$B_y^{(0)} = u_y^{(0)} = U_y^* - U_y^{\mathrm{N}} = -\frac{1}{(u_0 + 1)} \cdot y. \tag{3.24d}$$

3.5.2. South of the reconnection line. Corresponding properties valid south of the reconnection line are as follows.

Reconnection line at two Earth radii from the sub-solar point:

$$\eta \to -\infty: \quad B_z^{(0)} = R_{\mathrm{mp}} \sqrt{\frac{u_0}{u_0 + 1}} \tag{3.25a}$$

$$B_y^{(0)} = 0 \tag{3.25b}$$

$$\eta \to +\infty: \quad B_z^{(0)} = -R_{\mathrm{mp}} \sqrt{\frac{u_0}{u_0 + 1}} \tag{3.25c}$$

$$B_y^{(0)} = -u_y^{(0)} = U_y^{\mathrm{S}} - U_y^* = \frac{1}{(u_0 + 1)} \cdot y. \tag{3.25d}$$

https://doi.org/10.1017/S0022377805004149 Published online by Cambridge University Press

Reconnection line at seven Earth radii from the sub-solar point:

$$\eta \to -\infty: \quad B_z^{(0)} = \frac{1}{2} \cdot R_{\rm mp} \sqrt{\frac{u_0}{u_0+1}} \tag{3.26a}$$

$$B_y^{(0)} = 0 \tag{3.26b}$$

$$\eta \to +\infty: \quad B_z^{(0)} = -R_{\rm mp} \sqrt{\frac{u_0}{u_0+1}} \tag{3.26c}$$

$$B_y^{(0)} = -u_y^{(0)} = U_y^{\rm S} - U_y^* = \frac{1}{(u_0+1)} \cdot y. \tag{3.26d}$$

At the reconnection site $f_0 = u_z^{(0)}$ and $g_0 = u_y^{(0)}$. Explicit expressions for C_1 to C_4 are to be found in the Appendix.

3.6. Solutions to the higher-order term f_1

Having obtained the lowest order solutions it is straightforward to expand the right-hand side of (3.20c). This gives five different types of terms:

$$A_1 \cdot \mathrm{erf}(\eta) \tag{3.27a}$$

$$A_2 \cdot \mathrm{erf}(\sqrt{2}\eta) \tag{3.27b}$$

$$A_3 \eta \cdot e^{-2\eta^2} \tag{3.27c}$$

$$A_4 \eta \cdot e^{-\eta^2} \tag{3.27d}$$

$$A_5, \tag{3.27e}$$

where A_{1-5} are constants. We solve for each term and superpose. This results for f_1:

$$\begin{aligned} f_1 = &\left(-\sqrt{\pi} C_3 \cdot \eta^2 - \frac{1}{2}\sqrt{\pi} C_3 \right) \cdot \mathrm{erf}(\eta) \\ &+ \left(\sqrt{\pi} C_3 \cdot \eta^2 + \frac{1}{4}\sqrt{\pi} C_3 + \frac{Q_y C_2}{U_z^0} \right) \cdot \mathrm{erf}(\sqrt{2}\eta) \\ &+ \left(\frac{C_3}{\sqrt{2}} + \frac{3 C_2 Q_z}{\sqrt{2} U_z^0 \sqrt{\pi}} \right) \cdot \eta e^{-2\eta^2} - C_3 \cdot \eta e^{-\eta^2} \\ &- \frac{1}{2} \cdot \left(Q_z - \frac{Q_y C_1}{2 U_z^0} + C_4 \right), \end{aligned} \tag{3.28}$$

which, in turn, gives the velocities

$$u_y^{(0)} = C_4 - \frac{Q_y C_2}{U_z^0} \cdot \mathrm{erf}(\sqrt{2}\eta) + \frac{\sqrt{\pi} C_3}{2} \cdot \mathrm{erf}(\eta) \tag{3.29a}$$

$$\begin{aligned} u_z^{(0)} = &C_1 + C_2 \cdot \mathrm{erf}(\sqrt{2}\eta) + Z \cdot \left[\left(-\sqrt{\pi} C_3 \cdot \eta^2 - \frac{1}{2}\sqrt{\pi} C_3 \right) \cdot \mathrm{erf}(\eta) \right. \\ &+ \left(\sqrt{\pi} C_3 \cdot \eta^2 + \frac{1}{4}\sqrt{\pi} C_3 + \frac{Q_y C_2}{U_z^0} \right) \cdot \mathrm{erf}(\sqrt{2}\eta) \\ &+ \left(\frac{C_3}{\sqrt{2}} + \frac{3 C_2 Q_z}{\sqrt{2} U_z^0 \sqrt{\pi}} \right) \cdot \eta e^{-2\eta^2} \\ &\left. - C_3 \cdot \eta e^{-\eta^2} - \frac{1}{2} \cdot \left(Q_z - \frac{Q_y C_1}{2 U_z^0} + C_4 \right) \right]. \end{aligned} \tag{3.29b}$$

https://doi.org/10.1017/S0022377805004149 Published online by Cambridge University Press

4. Results

In this section we present the results treating the plasma flow during the transition from the magnetosheath to the magnetosphere, and the development of the magnetic field for different Z. We consider a solar wind velocity of 300 km s^{-1} corresponding to a Mach number in the solar wind equal to 6, and an interplanetary magnetic field of 18 nT. The solar wind plasma density is chosen as 5 cm^{-3}. Two different locations of the reconnection line are chosen; 2 and $7R_E$ from the sub-solar point, respectively.

4.1. Reconnection line at two Earth radii from the sub-solar point

4.1.1. The plasma flow during the transition from the magnetosheath to the magnetosphere. The total velocities in the y and z directions are:

$$U_y^* = u_y^{(0)} + U_y \tag{4.1a}$$

$$U_z^* = u_z^{(0)} + U_z, \tag{4.1b}$$

where $u_y^{(0)}$, $u_z^{(0)}$ and the DeHoffmann–Teller velocities are in accordance with (3.29) and (3.16), respectively. The development of the total velocity during the transition from the magnetosheath region to the magnetosphere is illustrated in the vector-field plot (see Fig. 2). Also compare with the results in Sec. 4.3, for the development of the magnitude of the plasma velocity during the transition. The field plots show mainly the direction of the flow, not the magnitude of the plasma velocity.

The reconnection line is in this case located at a distance of $2R_E$ along the magnetopause from the sub-solar point. The development of the flow is illustrated through four different values of η: $\eta = 3$, 0.4, 0.3 and -3. After the transition to the magnetosphere the plasma flow is mainly in the direction of the reconnected field lines. For the case of reconnection at the sub-solar point the plasma flow would be symmetrical around the reconnection line during the transition from the magnetosheath to the magnetosphere. As the magnetosheath velocity along the magnetopause increases further away from the sub-solar point, the effect of asymmetry is more distinct. Compare with Fig. 5 (in Sec. 4.2), representing the development of the plasma flow for a location of the reconnection line at $7R_E$ from the sub-solar point.

4.1.2. Development of the magnetic field for different Z. The relation between the lowest-order term of the velocity and the magnetic field is

$$\mathbf{B}_{0_N} = \mathbf{u}_0 \tag{4.2a}$$

$$\mathbf{B}_{0_S} = -\mathbf{u}_0 \tag{4.2b}$$

north and south of a reconnection line, respectively. The z-component of the magnetic field is plotted for four different Z; $Z = 0$, ± 0.175, ± 0.35 and ± 0.525, where the positive sign, as earlier, corresponds to the case north of the reconnection line. The development of this component of the magnetic field in the region stretching from $\eta = 3$ to -3 is presented in Fig. 3.

The development of the magnetic field is represented for $y = 0.1$–0.4. Recalling that $B_y^{(0)}$ scales linearly with y, the development of this magnetic field component for negative y is the mirror image of the corresponding development for positive y. Since $B_y^{(0)}$ is independent of Z, it is identical north and south of the reconnection line (see Fig. 4).

https://doi.org/10.1017/S0022377805004149 Published online by Cambridge University Press

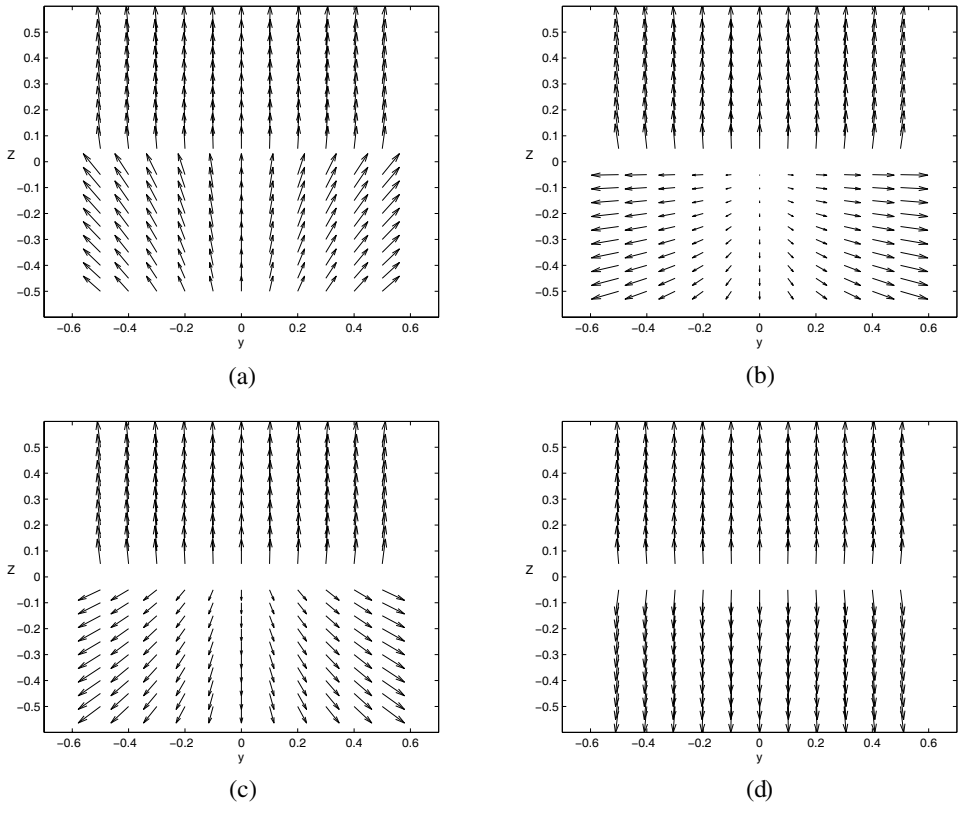


Figure 2. The plasma flow during the transition from the magnetosheath region to the magnetosphere: (a) $\eta = 3$, (b) $\eta = 0.4$, (c) $\eta = 0.3$ and (d) $\eta = -3$. η is the coordinate perpendicular to the tangent of the magnetopause, i.e. the re-scaled x-coordinate. Z is the coordinate perpendicular to η, having its origin at the reconnection line. The reconnection line is in this case located at $2R_{\mathrm{E}}$ from the sub-solar point.

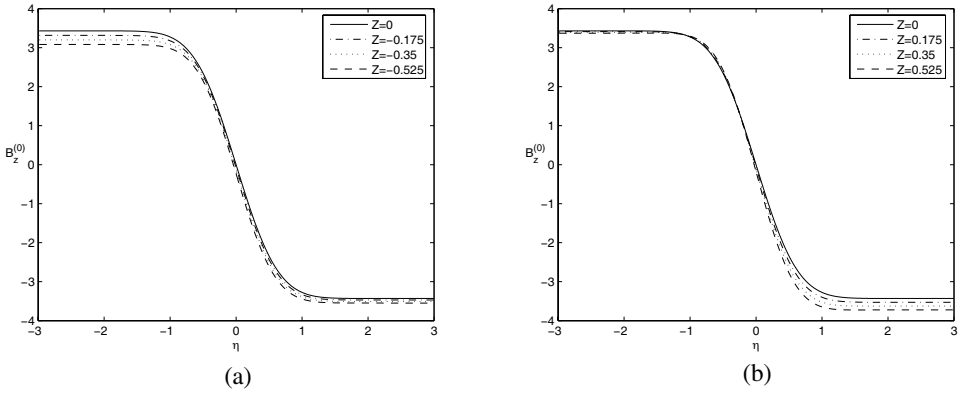


Figure 3. The Z-component of the magnetic field during the transition from the magnetosheath region to the magnetosphere, for different Z: (a) north of the reconnection line ($Z > 0$), (b) south of the reconnection line ($Z < 0$). The corresponding legends representing different Z values for the southern case are: solid, $Z = 0$; dash-dotted, $Z = -0.175$; dotted, $Z = -0.35$; dashed, $Z = -0.525$. There are corresponding yields for the northern case, but with Z being positive. Reconnection line at $2R_{\mathrm{E}}$ from the sub-solar point.

https://doi.org/10.1017/S0022377805004149 Published online by Cambridge University Press

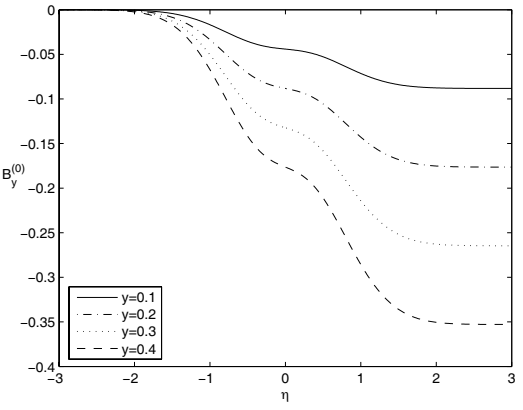


Figure 4. The y-component of the magnetic field during the transition from the magnetosheath region to the magnetosphere for different y. The corresponding legends representing different y values are: solid, $y = 0.1$; dash-dotted, $y = 0.2$; dotted, $y = 0.3$; dashed, $y = 0.4$. Since $B_y^{(0)}$ is independent of Z, it is identical north and south of the reconnection line. Reconnection line at $2R_E$ from the sub-solar point.

4.2. Reconnection line at seven Earth radii from the sub-solar point

4.2.1. The plasma flow during the transition from the magnetosheath to the magnetosphere. As for the case with the reconnection line located at the distance of $2R_E$ from the sub-solar point, the direction of the flow north of the reconnection line is constant through the transition from the magnetosheath to the magnetosphere. This because of the positive velocity gradient in the z-direction, resulting in a flow direction at the outer boundary ($\eta \to \infty$) of the magnetopause in alignment with the reconnected field line north of the reconnection line (see Fig. 5). See also Sec. 4.3 in addition, for the development of the plasma speed during the transition. The behavior of the flow pattern south of the reconnection line is more dramatic. As for the previous case, the outer flow south of the reconnection line is dominated by the positive gradient in the z-direction. During the transition to the magnetosphere, the flow is turned to be aligned with the reconnected field line, which is in the opposite direction to the outer flow. For the case of reconnection at the sub-solar point, the flow is symmetrical around the reconnection line. As the magnetosheath plasma velocity at the magnetopause boundary increases further away from the sub-solar point, the asymmetrical effect is stronger for reconnection at higher latitudes. The figures represents the flow at the same η location as for the previous case.

4.2.2. Development of the magnetic field for different Z. Due to the similar behavior for the z-component of the magnetic field as for the same component of the plasma velocity with a positive gradient in the z-direction, the magnitude of the magnetic field along the magnetopause increases when further away from the sub-solar point. The deviation from the initial distribution at $Z = 0$ is more distinct for reconnection at lower latitudes (compare Figs 6 and 3).

Since the y-component of the magnetic field is independent of Z, the effect is not as dramatic as for the z-component (see Figs 4 and 7). In contrast, as the z-component dominates the behavior, the y-component is weakened when reconnection occurs further away from the sub-solar point.

https://doi.org/10.1017/S0022377805004149 Published online by Cambridge University Press

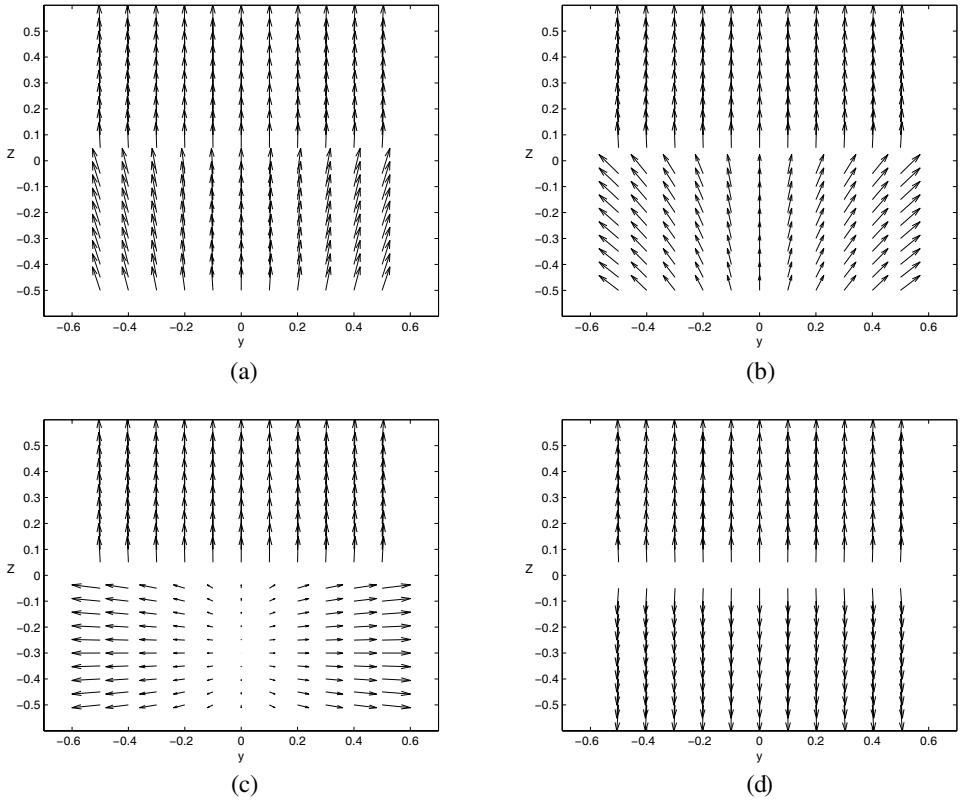


Figure 5. The plasma flow during the transition from the magnetosheath region to the magnetosphere: (a) $\eta = 3$, (b) $\eta = 0.4$, (c) $\eta = 0.3$ and (d) $\eta = -3$. η is the coordinate perpendicular to the tangent of the magnetopause, i.e. the re-scaled x-coordinate. Z is the coordinate perpendicular to η, having its origin at the reconnection line. In this case the reconnection line is located at $7R_{\mathrm{E}}$ from the sub-solar point.

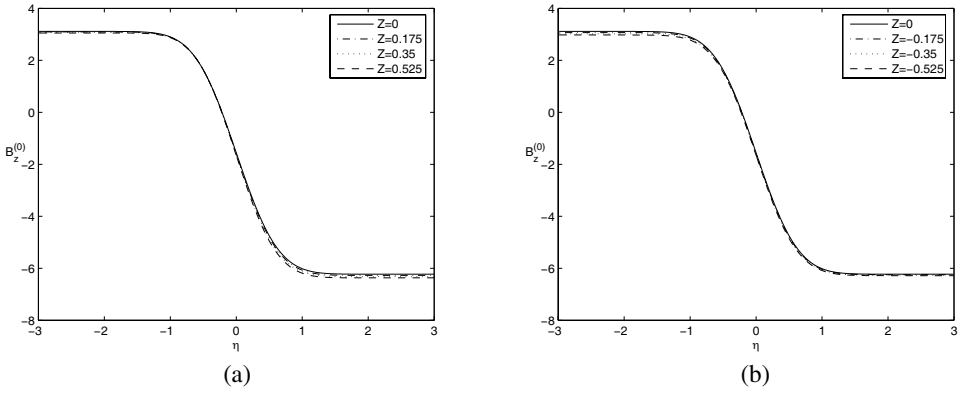


Figure 6. The Z-component of the magnetic field during the transition from the magnetosheath region to the magnetosphere, for different Z: (a) north of the reconnection line ($Z > 0$), (b) south of the reconnection line ($Z < 0$). The corresponding legends representing different Z values for the southern case are: solid, $Z = 0$; dash-dotted, $Z = -0.175$; dotted, $Z = -0.35$; dashed, $Z = -0.525$. Corresponding yields for the northern case, but with Z being positive. Reconnection line at $7R_{\mathrm{E}}$ from the sub-solar point.

https://doi.org/10.1017/S0022377805004149 Published online by Cambridge University Press

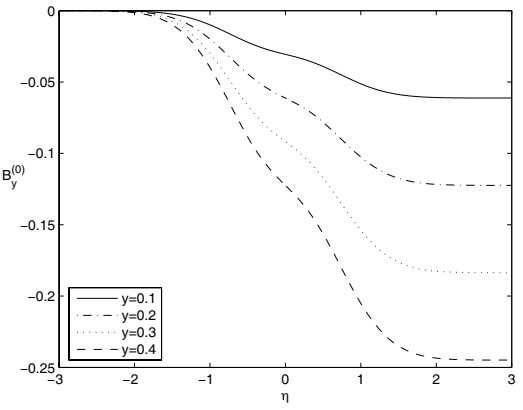


Figure 7. The y-component of the magnetic field during the transition from the magnetosheath region to the magnetosphere for different y. The corresponding legends representing different y values are: solid, $y=0.1$, dash-dotted, $y=0.2$; dotted, $y=0.3$; dashed, $y=0.4$. Since $B_y^{(0)}$ is independent of Z, it is identical north and south of the reconnection line. Reconnection line at $7R_E$ from the sub-solar point.

4.3. Development of the magnitude of the plasma velocity

The development of the magnitude of the plasma velocity during the transition from the magnetosheath to the magnetosphere is represented by Fig. 8. We consider as previously in the analysis two locations of the reconnection line ($y=0.2$ for all cases). Z varies from 0 to 0.525 in positive (northern case) and negative directions (southern case). North of the reconnection line the development of the plasma speed is quite stable with a constant acceleration during the transition. For the case with the reconnection line located at $7R_E$ from the sub-solar point, the acceleration is higher due to a greater increase in the velocity at the outer magnetopause boundary than is the case for reconnection closer to the sub-solar point.

South of the reconnection line the behavior is not as structured due to the change of direction for the flow south of the reconnection line during the transition. The plasma speed is actually decreased during the transition close to the current sheet – an event which is more distinct for reconnection at higher latitudes. The effect is caused by the turnover the plasma flow is exposed to when passing through the magnetopause. At the outer boundary the plasma velocity is dominated by the direction towards positive Z, an effect which is stronger further away from the sub-solar point.

5. Summary and conclusions

In this paper a three-dimensional analysis of the solar wind flow in the magnetosheath, combined with a boundary flow separated by a thin transition layer, is presented. A curvilinear coordinate system is used, where at the sub-solar point; x is the coordinate pointing towards the sun, z the coordinate lying in the tangential direction of the magnetopause, and with y completing the right-handed system. Magnetic reconnection off the sub-solar point is considered. Reconnection is assumed to occur along a line located north of the sub-solar point, where z is constant and y varies. The basis of the analysis is the MHD equations including dissipative

https://doi.org/10.1017/S0022377805004149 Published online by Cambridge University Press

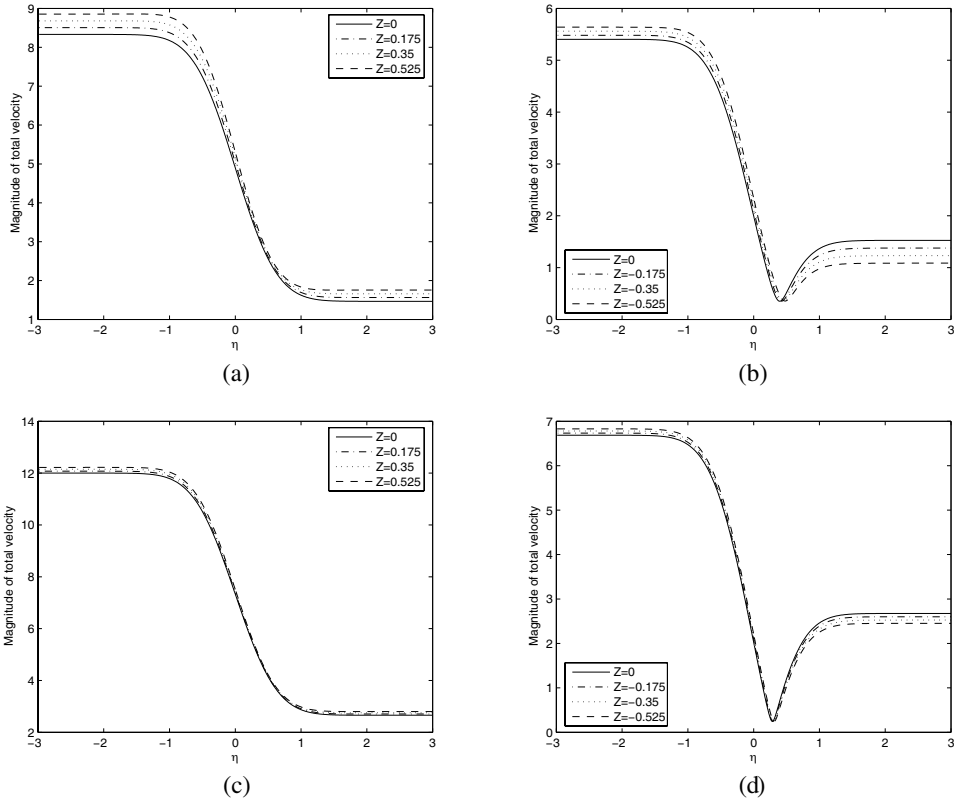


Figure 8. Development of the absolute velocity during the transfer from the magnetosheath to the magnetosphere for different Z: (a) north of the reconnection line, located at $2R_{\mathrm{E}}$ from the sub-solar point; (b) south of the reconnection line, with location as in (a); (c) north of the reconnection line, located at $7R_{\mathrm{E}}$ from the sub-solar point; (d) south of the reconnection line, with location as in (c). Corresponding legends are solid, $Z=0$; dash-dotted, $Z=\pm 0.175$; dotted, $Z=\pm 0.35$; dashed, $Z=\pm 0.525$. The minus sign corresponds to the southern case. $y=0.2$ for all cases.

effects such as viscosity and resistivity. Considering the transition layer to be very thin, the equations can be solved approximately by using a perturbation expansion for large Reynolds and Lundqvist numbers. The perturbation expansion results in simplified equations describing the resolution of the transition layer, separating the magnetosheath plasma from the boundary layer plasma. The equations treat the case with a varying magnetosheath flow. In this paper the outer flow is specified as linearly increasing from the sub-solar point, where the velocity gradient in the z-direction is a function of the location of the reconnection line. This results in two characteristic solutions: one describing the properties north of the reconnection line and the other describing the properties south of the reconnection line. The velocity of the plasma flow is higher for the case north of the reconnection line. Two cases of the location of the reconnection line are treated: at 2 and $7R_{\mathrm{E}}$, respectively. The development of the plasma flow, the magnitude of the plasma velocity and the magnetic field during the transition from the magnetosheath region to the magnetosphere are presented. For the case of reconnection off the

https://doi.org/10.1017/S0022377805004149 Published online by Cambridge University Press

sub-solar point, the plasma flow velocity is higher north of the reconnection line. This is due to the positive velocity gradient along the magnetopause boundary. For reconnection at higher latitudes the difference between the evolution of the velocities for the northern and southern cases are more distinct, due to the higher magnetosheath plasma velocity. The evolution of the magnetic field north and south of the reconnection line during the transition for the case of a higher latitude reconnection line is also more finite. The magnitude of the z-component for the magnetic field is also higher, while the y-component is weakened for reconnection further away from the sub-solar point.

There are several ideas of how to continue the present work. Work treating compressible effects with a variable density of the magnetosheath plasma has been initiated. Up to now we have focused on viscosity and resistivity as the only non-ideal effects. A natural extension of the analysis would be to include other terms in the generalized Ohm's law. Finally, a comparison between the theoretical model(s) and observational data is of great interest and importance.

Acknowledgements

This work is financed through the Swedish National Graduate School of Space Technology. LGW thanks E. N. Davidsson for valuable help during the work with this paper.

Appendix A. Constants C_1 to C_4 for each case

In this Appendix we present the explicit expressions for C_1 to C_4 for each location of the reconnection line.

North of the reconnection line:

$$C_1^{(2)} = 0 \tag{A 1a}$$

$$C_2^{(2)} = -R_{\mathrm{mp}}\sqrt{\frac{u_0}{u_0+1}} \tag{A 1b}$$

$$C_3^{(2)} = -\frac{2Q_y R_{\mathrm{mp}}\sqrt{u_0/(u_0+1)}}{U_z^0\sqrt{\pi}} - \frac{1}{\sqrt{\pi}(u_0+1)} \tag{A 1c}$$

$$C_4^{(2)} = -\frac{1}{2(u_0+1)} \tag{A 1d}$$

$$C_1^{(7)} = -\frac{R_{\mathrm{mp}}}{4}\sqrt{\frac{u_0}{u_0+1}} \tag{A 1e}$$

$$C_2^{(7)} = -\frac{3R_{\mathrm{mp}}}{4}\sqrt{\frac{u_0}{u_0+1}} \tag{A 1f}$$

$$C_3^{(7)} = -\frac{3Q_y R_{\mathrm{mp}}\sqrt{u_0/(u_0+1)}}{2U_z^0\sqrt{\pi}} - \frac{1}{\sqrt{\pi}(u_0+1)} \tag{A 1g}$$

$$C_4^{(7)} = -\frac{1}{2(u_0+1)}, \tag{A 1h}$$

where the indices (2) and (7) represents the two different locations of the reconnection line.

https://doi.org/10.1017/S0022377805004149 Published online by Cambridge University Press

South of the reconnection line:

$$C_1^{(2)} = 0 \tag{A 2a}$$

$$C_2^{(2)} = R_{\mathrm{mp}}\sqrt{\frac{u_0}{u_0+1}} \tag{A 2b}$$

$$C_3^{(2)} = \frac{2Q_y R_{\mathrm{mp}}\sqrt{u_0/(u_0+1)}}{U_z^0\sqrt{\pi}} + \frac{1}{\sqrt{\pi}(u_0+1)} \tag{A 2c}$$

$$C_4^{(2)} = \frac{1}{2(u_0+1)} \tag{A 2d}$$

$$C_1^{(7)} = \frac{R_{\mathrm{mp}}}{4}\sqrt{\frac{u_0}{u_0+1}} \tag{A 2e}$$

$$C_2^{(7)} = \frac{3R_{\mathrm{mp}}}{4}\sqrt{\frac{u_0}{u_0+1}} \tag{A 2f}$$

$$C_3^{(7)} = \frac{3Q_y R_{\mathrm{mp}}\sqrt{u_0/(u_0+1)}}{2U_z^0\sqrt{\pi}} + \frac{1}{\sqrt{\pi}(u_0+1)} \tag{A 2g}$$

$$C_4^{(7)} = \frac{1}{2(u_0+1)}. \tag{A 2h}$$

References

Axford, W. I. 1964 Viscous interaction between the solar wind and the Earth's magnetosphere. *Planet. Space Sci.* **12**, 45–53.

Biernat, H. K., Heyn, M. F., Kubyshkin, I. V. and Semenov, V. S. 1983 Field line reconnexion in the two-dimensional asymmetric case. *J. Plasma Phys.* **30**, 321–344.

Büchner, J. and Kuska, J. P. 1997 Numerical simulation of three-dimensional reconnection due to the instability of collisionless current sheets. *Adv. Space Res.* **19**(12), 1817–1822.

Chapman, S. and Ferraro, V. C. A. 1931 A new theory of magnetic storms, Part I. The initial phase. *Terr. Mag. Atmos. Elect.* **36**, 7.

Cowley, S. W. H. 1976 Comments on the merging of non-antiparallel magnetic fields. *J. Geophys. Res.* **81**, 3455.

Cowley, S. W. H. 1995 Theoretical perspectives of the magnetopause. In: *Physics of the Magnetopause, Geophys. Monogr. Ser.* vol. 90 (ed. P. Song, B. U. Ö. Sonnerup and M. F. Thomsen). Washington, DC: AGU, pp. 29–43.

Cowley, S. W. H. and Owen, C. J. 1989 A simple illustrative model of open flux tube motion over the dayside magnetopause. *Planet. Space Sci.* **37**, 1461.

DeHoffmann, F. and Teller, E. 1950 Magnetohydrodynamic shocks. *Phys. Rev. Lett.* **80**, 692.

Dungey, J. W. 1961 Interplanetary magnetic field and the auroral zones. *Phys. Rev. Lett.* **6**, 47.

Dungey, J. W. 1995 Origins of the concept of reconnection and its applications to the magnetopause: a historical view. In: *Physics of the Magnetopause, Geophys. Monogr. Ser.* vol. 90 (ed. P. Song, B. U. Ö. Sonnerup and M. F. Thomsen). Washington, DC: AGU, pp. 17–19.

Greene, J. M. 1988 *J. Geophys. Res.* **93**, 8583–8590.

Farrugia, C. J. et al. 1998 Charts of joint Kelvin–Helmholz and Rayleigh–Taylor instabilities at the dayside magnetopause for strongly northward interplanetary magnetic field. *J. Geophys. Res.* **103**, 6703–6728.

Haerendel, G., Paschmann, N., Sckoke, N. and Rosenbauer H. 1978 The front side boundary layer of the magnetosphere and the problem of reconnection. *J. Geophys. Res.* **83**, 3195.

Hesse, M. and Schindler, K. 1988 *J. Geophys. Res.* **93**, 5547–5557.

https://doi.org/10.1017/S0022377805004149 Published online by Cambridge University Press

Heyn, M. F., Biernat, H. K., Semenov, V. S. and Kubyshkin, I. V. 1985 Dayside magnetopause reconnection. *J. Geophys. Res.* **90**, 1781–1785.

Merrill, R. T., McElhinny, M. W. and McFadden, P. L. 1996 The magnetic field of the Earth. In: *Int. Geophys. Series*, vol. 63. San Diego, CA: Academic Press, p. 58.

Parker, E. N. 1957 Sweet's mechanism for merging megnetic fields in conducting fluids. *J. Geophys. Res.* **62**, 509.

Petschek, H. E. 1964 Magnetic field annihilation. In: *AAS–NASA Symp. on the Physics of Solar Flares, NASA Spec. Publ., SP-50*, vol. 425, pp. 425–439.

Priest, E. R. 1997 Three-dimensional magnetic reconnection in the solar corona. *Phys. Plasmas* **4**(5), 1945–1952.

Priest, E. R. 2003 Theory of 3D reconnection and coronal heating. *Adv. Space Res.* **32**(6), 1021–1027.

Priest, E. R. and Forbes, T. G. 1986 New models for fast steady state magnetic reconnection. *J. Geophys. Res.* **91**, 5579.

Priest, E. R. and Forbes, T. G. 1989 Steady magnetic reconnection in three dimensions. *Solar Phys.* **119**, 211–214.

Sonnerup, B. U. Ö. 1970 Magnetic-field re-connexion in a highly conducting incompressible fluid. *J. Plasma Phys.* **4**, 161–174.

Sonnerup, B. U. Ö. 1979 Magnetic field reconnection. In: *Solar System Plasma Physics*, vol. III, chap. 3, sec. 1.2. (ed. L. Lanzerotti, C. Kennel and E. N. Parker). Amsterdam: North-Holland.

Spreiter, J. R. and Stahara, S. 1980 A new predictive model for determining solar wind terrestrial planet instructions. *J. Geophys. Res.* **85**, 6769.

Sweet, P. A. 1958 The neutral point theory of solar flares. In: *Proc. Int. Astronomical Union Symp. on Electromagnetic Phenomena in Cosmical Physics*, No. 6, Stockholm, 1956. Cambridge: Cambridge University Press, pp. 123–134.

Ugai, M. 1991 Computer modelling of three-dimensional dynamics. *J. Plasma Phys.* **45**(2), 251–266.

Ugai, M., Kondoh, K. and Shimizu, T. 2003 Computer studies on the three-dimensional spontaneous fast reconnection models as a nonlinear instability. *Phys. Plasmas* **11**(4), 1416–1423.

Vasyliunas, V. M. 1975 Theoretical models of magnetic field line merging. *Rev. Geophys.* **13**, 303–336.

Wang, Y. L., Raeder, J. and Russell, C. T. 2004 Plasma depletion layer: magnetosheath flow structure and forces. *Ann. Geophys.* **22**, 1001–1017.

Westerberg, L. G. and Åkerstedt, H. O. 2005 A two dimensional analysis of the flow past an open terrestrial magnetopause. *J. Plasma Phys.* **71**(5). 1–26.

Yeh, T. and Axford, W. I. 1970 On the re-connexion of magnetic field lines in conducting fluids. *J. Plasma. Phys.* **4**, 207–229.

https://doi.org/10.1017/S0022377805004149 Published online by Cambridge University Press